Pergamon

Int. J. Heat Mass Transfer. Vol. 38, No. 13, pp. 2489–2500, 1995

0017-9310/95 $9.50+0.00

0017-9310(94)00342-4

Penetrative convection in a stably stratified enclosure

ABDULKARIM H. ABIB† and YOGESH JALURIA

Department of Mechanical and Aerospace Engineering, Rutgers, The State University of New Jersey, New Brunswick, NJ 08903, U.S.A.

(*Received* 17 *February* 1994 *and in final form* 26 *October* 1994)

Abstract—The penetrative convection induced by a localized heat source at the bottom surface of a partially open enclosure with a stably, thermally stratified ambient medium is studied using a finite-difference method. The stratification that is considered here is a stable two-layered temperature variation. This flow is of interest in many thermal processes such as enclosure fires. The influence of the stratification on the flow is examined. The convective motion occurring in the unstable lower-layer is found to penetrate significantly into the stable upper-layer only for a weak stratification. But small penetration occurs at large stratification levels. In addition, the flow field reveals a multi-cellular pattern and the penetrative motion occurs in the form of nearly horizontal motion in the lowest part of the stable upper-layer. The thermal field is studied in detail and other important details on this penetrative convective transport are brought out.

1. INTRODUCTION

Penetrative convection is defined as the process whereby convective motion arising in a stable region penetrates into an adjacent fluid layer which is stably stratified [1]. The study of penetrative convection is of importance in a wide variety of flows in the environment and in engineering applications. Some common geophysical and engineering examples include: the growth of a turbulent atmospheric boundary layer during early morning heating in the absence of wind; the mixing at the thermocline‡ due to the discharge of a buoyant jet from a power plant heat rejection system; and the terminal height of a buoyancy-induced rise of smoke and other combustion products in an enclosure fire due to the presence of stable, thermal stratification in the ambient medium.

In this paper, we focus our attention on the last example and consider penetrative convection in a stably, thermally stratified enclosure. This problem is very important in the prediction of movement of smoke in buildings. In fact, in enclosure fires, the mixing caused by the penetrative convection will affect the height of the hot–cold interface between the hot combustion products and lower region containing the inflow of cold air. This will, in turn, influence the fire-fighting and rescue operations, as well as the fire detection, control and extraction systems for smoke and other toxic gases [2].

A considerable amount of work has been done over the past three decades on external flows such as plumes and boundary layers in the presence of a stable, thermal ambient stratification. The results have been summarized by Turner [1], Jaluria [3] and List [4]. On the other hand, results for cavity flows with stratification are much less extensive, but include the studies of Walin [5], Chen *et al.* [6] and Torrance [7]. Numerical and experimental results on vented or partially open cavities and on the flow interaction with stably stratified ambient media are essentially non-existent. Therefore, in the present study, our efforts are directed at addressing this issue. We will limit our focus on the initial stages of fire growth where convective transport is the dominant energy transport mode. The influence of the stratification on the flow is examined. The penetration distance, velocity and temperature distributions, heat transfer results, and mass outflow rates are presented to quantify the penetrative convection that arises. It is found that for a weaker stratification level the thermal plume reaches the ceiling. But for a stronger level it is unable to penetrate into the stable upper-layer. Therefore, such failure of the fire plume to reach the upper region of a room could result in a significant alteration of the transport processes.

2. ANALYSIS

2.1. *The problem of interest*

Penetrative convection in an enclosure, where the background ambient medium is stably and thermally stratified, is considered. A two-dimensional rectangular cavity with a partially open side is examined. It is heated by a localized energy source with a con-

† Present address: Center for Great Lakes Studies, University of Wisconsin-Milwaukee, 600 E. Greenfield Ave, Milwaukee, WI 53204-2944, U.S.A.

‡ A layer in a thermally stratified body of water in which the temperature decreases with depth.

NOMENCLATURE

A	aspect ratio, L/H
Gr	Grashof number based on the height of the cavity, $g\beta(Q_0/\kappa)H^3/\nu^2$
g	magnitude of the gravitational acceleration
H	height of the compartment
H_i, h_i	height of the interface, $h_i = H_i/H$
H_0, h_0	height of the opening, $h_0 = H_0/H$
L	length of the compartment
L_e, l_e	length of the extended computational domain (ECD), $l_e = L_e/H$
L_s, l_s	length of the heat source, $l_s = L_s/H$
L_t, l_t	thickness of the doorway soffit, $l_t = L_t/H$
$\dot{m}$	dimensionless mass outflow rate at compartment opening
N_b	buoyancy or Brunt–Vaisala frequency
N_0	computed frequency of the peroidic motion
$\overline{Nu}_s$	average Nusselt number over the heat source defined in equation (22)
Pr	Prandtl number, ν/α
S	stratification parameter, $\Delta T_i/\Delta T_q$
Q_0	total heat input by the source per unit width
$\dot{q}''_o$	total heat input per unit area of the source, Q_0/L_s
t	dimensionless time
t_b	Brunt–Vaisala time scale
Δt	dimensionless time step
T	temperature
ΔT_i	ambient temperature rise
ΔT_q	characteristic temperature difference, Q_0/κ
u	dimensionless velocity components in the x axis
v	dimensionless velocity components in the y axis
X, x	horizontal coordinate, $x = X/H$
X_{max}	length of the computational domain ($X_{max} = L + L_e$)
x_{max}	dimensionless length of the computational domain ($x_{max} = X_{max}/H$)
X_s, x_s	distance between the heat source and the back wall, $x_s = X_s/H$
Y, y	vertical coordinate, $y = Y/H$
Z_i	dimensionless height of hot–cold interface.

Greek symbols

α	thermal diffusivity
β	coefficient of thermal expansion, $\beta = 1/T$ for perfect gas
Γ	ambient temperature gradient defined in equation (2)
γ	dimensionless ambient temperature gradient defined in equation (3)
δ_p	dimensionless penetration height of the thermal plume
ζ	dimensionless vorticity
Θ	dimensionless temperature, $T - T_{\infty,y}/\Delta T_q$
κ	coefficient of thermal conductivity
ν	kinematic viscosity
ρ	density
φ	dimensionless temperature, $T - T_{\infty,0}/\Delta T_q = \Theta + T_{\infty,y} - T_{\infty,0}/\Delta T_q$
ψ	dimensionless stream function.

Subscripts

i	hot–cold interface
max	maximum value
s	heat source or fire
w	wall value
∞,0	ambient value at the lower-layer ($y = 0$) in two-layer system
∞,u	ambient value at the upper-layer in a two-layer system
∞,y	ambient value at the vertical location y.

stant heat input per unit width, Q_0, at the bottom boundary. The aspect ratio of the cavity is held constant at a value of 2 which is typical of room-size enclosures. The cavity is in communication with a long corridor through the opening, see Fig. 1(a). The corridor surrounding the opening is considered to be stably stratified due to the thermal energy input from various sources such as a fire at the far end of the corridor or in an adjacent room. The stratification of the environment far away from the cavity is maintained essentially unaltered over the course of the experiment as long as there is an energy input. In modeling the environmental conditions, a two-layer temperature distribution divided by a sharp interface is particularly appropriate. This is usually encountered in room fires, where a hot upper layer lies above a relatively cooler lower layer, see Cooper *et al.* [8].

In this paper only laminar regime is considered. Turbulent flow study is reported by Abib [9]. This model, despite assuming two-dimensional, laminar flow, gives results that shed light on the effects of stratification on the growth and spread of fire in a room. Furthermore, it is already clear from studies of turbulent flows that a strong stable thermal stratification causes the flow to re-laminarize.

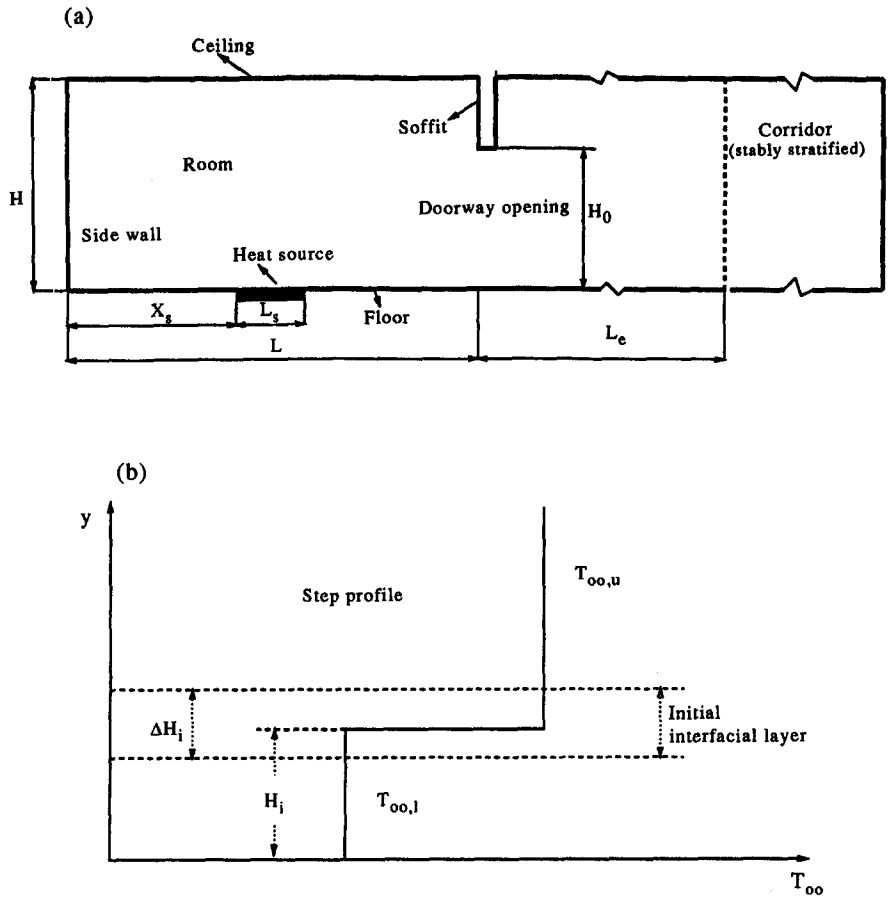

Fig. 1. (a) Room and corridor regions with a step ambient temperature stratification. (b) A two-layer ambient temperature variation.

2.2. *Ambient temperature variation*

When considering the two-layer ambient temperature variation, Fig. 1(b), a step-change interface is physically not reasonable and the temperature jump at the interface is approximated by a gradual rise, using the following expression

$$T_{\infty,y} = 0.5\Delta T_i\left\{1+\tanh\left[b\left(\frac{Y}{H}-\frac{H_i}{H}\right)\right]\right\} \quad (1)$$

where ΔT_i is the maximum temperature difference across the interface, H_i is the height of the interface, H is the height of the enclosure, and b is a specified constant. Because of smoothing of the step profile, an interfacial layer is created with a width given as $\Delta H_i = 2Hb^{-1}$. The smaller the interfacial layer, the better is the approximation to a step profile becomes. By varying the constant factor b we can approximate the ambient temperature profile satisfactorily. For the present problem, besides the interface temperature rise ΔT_i, there is another characteristic temperature difference $\Delta T_q = Q_0/\kappa$ which can be obtained from the ratio between the total heat input per unit width Q_0 and the thermal conductivity of the fluid κ. Thus, the ratio between these two characteristic temperature differences (ΔT_i and ΔT_q) defines an important number called stratification parameter S which quantifies the importance of effects of ambient temperature stratification for a given energy input level. The ambient temperature gradient Γ is defined as:

$$\Gamma = \frac{dT_{\infty,y}}{dY} = \frac{0.5b}{H}\Delta T_i \operatorname{sech}^2\left[b\left(\frac{Y}{H}-\frac{H_i}{H}\right)\right] \quad (2)$$

whereas, the corresponding dimensionless ambient temperature gradient γ is defined by the following expression as:

$$\gamma = \frac{H}{\Delta T_q}\Gamma = 0.5b\frac{\Delta T_i}{\Delta T_q}\operatorname{sech}^2\left[b\left(\frac{Y}{H}-\frac{H_i}{H}\right)\right]$$

$$= 0.5bS\operatorname{sech}^2\left[b\left(\frac{Y}{H}-\frac{H_i}{H}\right)\right]. \quad (3)$$

2.3. *Governing equations*

The governing equations expressing the conservation of mass, momentum and energy, for an incompressible Boussinesq fluid, can be written in dimensionless form as [3]:

$$u = \frac{\partial\psi}{\partial y} \quad v = -\frac{\partial\psi}{\partial x} \quad (4)$$

$$\frac{\partial^2\psi}{\partial x^2}+\frac{\partial^2\psi}{\partial y^2}=-\zeta \tag{5}$$

$$\frac{\partial\zeta}{\partial t}+\frac{\partial(u\zeta)}{\partial x}+\frac{\partial(v\zeta)}{\partial y}=\frac{1}{\sqrt{Gr}}\left\{\frac{\partial}{\partial x}\left(\frac{\partial\zeta}{\partial x}\right)+\frac{\partial}{\partial y}\left(\frac{\partial\zeta}{\partial y}\right)\right\}+\frac{\partial\Theta}{\partial x} \tag{6}$$

$$\frac{\partial\Theta}{\partial t}+\frac{\partial(u\Theta)}{\partial x}+\frac{\partial(v\Theta)}{\partial y}+v\gamma=\frac{1}{Pr\sqrt{Gr}}\left\{\frac{\partial}{\partial x}\left(\frac{\partial\Theta}{\partial x}\right)+\frac{\partial}{\partial y}\left(\frac{\partial\Theta}{\partial y}\right)+\frac{\mathrm{d}^2(T_{\infty,y}/\Delta T_q)}{\mathrm{d}y^2}\right\}. \tag{7}$$

Here, x and y are the dimensionless horizontal and vertical coordinate distances, u and v are the corresponding velocity components, t is the dimensionless time, ψ and ζ are the dimensionless stream function and vorticity. Θ is the dimensionless temperature with reference to ambient temperature value at the vertical location y and it is defined as:

$$\Theta=\frac{T-T_{\infty,y}}{\Delta T_q} \tag{8}$$

The dimensionless temperature can also be defined with reference to a fixed temperature value at $y=0$ (or the lower-layer in the two-layer ambient temperature variation). Let us denote this temperature by φ and its relationship to Θ is given as:

$$\varphi=\frac{T-T_{\infty,0}}{\Delta T_q}=\Theta+\frac{T_{\infty,y}-T_{\infty,0}}{\Delta T_q}. \tag{9}$$

The two temperature definitions are equivalent. The use of definition of Θ makes the boundary conditions for the energy equation much simpler to impose. However, an extra term $v\gamma$ appears in the energy equation (7) since the dimensionless temperature Θ is defined relative to the ambient temperature $T_{\infty,y}$ which is a function of y. This extra term in the equation describes the vertical convection in a stratified medium. In an isothermal ambient case, $T_{\infty,y}$ is constant and the extra term becomes zero. On the other hand, the dimensionless temperature φ which is defined relative to a constant value ($T_{\infty,0}$) is used in the presentation of the results in order to see temperature level above the lowest ambient temperature value.

Besides the dimensionless number S, the governing equations introduce two additional dimensionless parameters: the Grashof number Gr and the Prandtl number Pr, defined as:

$$Gr=\frac{g\beta\Delta T_q H^3}{\nu^2}\qquad Pr=\frac{\nu}{\alpha} \tag{10}$$

where g is the magnitude of gravitational acceleration, β is the coefficient of thermal expansion of the fluid, ν is the kinematic viscosity and α is the thermal diffusivity. H is the height of the cavity. Since the fluid considered is air, the Prandtl number Pr is set to a value of 0.72 for normal room temperatures. The parameters of the problem is then reduced to two, namely S and Gr.

The aspect ratio (length by height) A is held constant at a value of 2 (typical of room fires). The size of the heat source is also fixed ($L_s=0.2H$). The location of the heat source is taken as the middle of the bottom surface ($X_s=0.9H$). The location of the stable layer interface is also fixed ($H_i=0.5H$) for the calculations. Other values besides these typical values were also considered, but the basic trends obtained were found to be the same as those presented at these typical values.

2.4. *Initial and boundary conditions*

The cavity and the surrounding environment are considered to be initially stratified and quiescent. After the onset of the fire, the environment at the far end of the corridor is assumed to remain stably stratified. The initial and boundary conditions for the governing equations (5)–(7) are specified as

Initial condition at $t<0$

$$u=v=\psi=\zeta=\Theta=0\quad 0\leqslant x\leqslant x_{\max}\text{ and }0\leqslant y\leqslant 1. \tag{11}$$

Boundary conditions at $t\geqslant 0$

1. Bottom boundary (floor) at $y=0$:

$$u=v=\psi=0\quad \zeta=\zeta_w\quad 0\leqslant x\leqslant x_{\max} \tag{12}$$

$$\frac{\partial\Theta}{\partial y}=\begin{cases}0 & 0\leqslant x\leqslant x_s\\ \dot{q}''_o=\dfrac{1}{l_s} & x_s\leqslant x\leqslant x_s+l_s\\ 0 & x_s+l_s\leqslant x\leqslant x_{\max}.\end{cases} \tag{13}$$

2. Ceiling at $y=1$ and doorway soffit at $y=h_0$:

$$u=v=\psi=\frac{\partial\Theta}{\partial y}=0\quad \zeta=\zeta_w\quad 0\leqslant x\leqslant x_{\max}. \tag{14}$$

3. Left side wall or back wall at $x=0$:

$$u=v=\psi=\frac{\partial\Theta}{\partial x}=0\quad \zeta=\zeta_w\quad 0\leqslant y\leqslant 1. \tag{15}$$

4. Door soffit walls at $x=A$ and $x=A+l_t$:

$$u=v=\psi=0\quad \zeta=\zeta_w\quad \frac{\partial\Theta}{\partial x}=0\quad h_0\leqslant y\leqslant 1. \tag{16}$$

5. Right far-field boundary at $x=x_{\max}$:

$$v=\frac{\partial u}{\partial x}=\frac{\partial\psi}{\partial x}=\frac{\partial\zeta}{\partial x}=0\quad 0\leqslant y\leqslant 1 \tag{17}$$

$$\begin{cases}\Theta=0 & \text{if } u\leqslant 0\quad\text{(inflow)}\\ \dfrac{\partial\Theta}{\partial x}=0 & \text{if } u>0\quad\text{(outflow).}\end{cases} \tag{18}$$

The far-field boundary at $x = x_{max}$ is both an inflow and outflow boundary. At the bottom part of this boundary, a cooler inflow is established since the thermal plume rising over the source entrains fluid from the opening. On the top part of the boundary, instead, hot gases flow out. Therefore, the thermal boundary conditions should accommodate this physical condition. One way to do this is to apply condition (18) together with condition (17). This allows (i) the inflow to be at the temperature that exists at ambient medium and (ii) the outflow to take any temperature value since upwind conditions ($\partial\Theta/\partial x$) prevail.

2.5. *Numerical method*

The governing equations are discretized with the control-volume based finite-difference method, see [9] for details. The advection–diffusion terms are discretized with a power-law scheme [10]. The unsteady parabolic equations for transport of energy and vorticity is solved by an alternating line-by-line method. This method, like the Alternating Direct Implicit (ADI) techniques [11, 12] has a good stability properties, second-order accuracy in time and easy solution by inversion of tridiagonal matrices. On the other hand, the Poisson equation for the stream function is solved at each time step by the Successive Over Relaxation (SOR) method. The different transport equations for the dependent variables Θ, ζ and ψ are coupled in many different ways. Furthermore, the nonlinearities in advection terms and in the source terms also provide further coupling of the dependent variables. Instead of fully linearizing the transport equations by using the Newton–Raphson method, the coupling and the nonlinearities are treated iteratively at each time step. The iterative method is a double loop in which the inner loops are a line by line method for the variables Θ and ζ and a SOR method for the ψ variable. The iterative method is terminated after convergence based on the criteria that the change or relative error in the dependent variables produced by successive iterations is reduced below a prescribed small value (say 10^{-5}). At same time the normalized residual sources of the finite difference equations is also reduced below a prescribed small value (10^{-2}–10^{-3}).

The existence of the boundary layer near the walls requires that a non-uniform grid be used that gives a strong grid refinement along the walls. A hyperbolic grid distribution is employed, with the grid points given by

$$\frac{X_i}{H} = \frac{1}{2}\left\{1 + \frac{\tanh\left[\alpha_1\left(i/i_{max} - \frac{1}{2}\right)\right]}{\tanh\left(\alpha_1/2\right)}\right\} \qquad i = 0, 1, 2, \ldots, i_{max} \quad (19)$$

$$\frac{Y_i}{H} = \frac{1}{2}\left\{1 + \frac{\tanh\left[\alpha_1\left(i/i_{max} - \frac{1}{2}\right)\right]}{\tanh\left(\alpha_1/2\right)}\right\} \qquad i = 0, 1, 2, \ldots, i_{max} \quad (20)$$

where α_1 is given by $\alpha_2 = \alpha_1/\sinh(\alpha_1)$. After extensive numerical testing, α_2 is taken as 1.5×10^{-3}, which gives $\alpha_1 = 6.811$, to ensure that at least eight to 10 points lie between the wall and the location of maximum velocity. In the y-direction, extra grid points are added at the location of the interface $(H_i - \frac{1}{2}\Delta H_i \leqslant Y \leqslant H_i + \frac{1}{2}\Delta H_i)$ in order to resolve sharp temperature gradients. Also, in the x-direction, extra points (10 points) are added at the location of the heat source $(X_s \leqslant X \leqslant X_s + L_s)$.

The time evolution in the open cavity in the presence of stable thermal stratification is dominated by Brunt–Vaisala time scale $t_b = H^2/\alpha(SGrPr^2)^{-1/2}$ and determines the maximum time step that gives a stable numerical solution. This time step limitation has also been reported by Jones [13], Thompson *et al.* [14] and Henkes [15] in their study of buoyancy-driven turbulent flow in a rectangular cavity. For most of the cases, a time step $\Delta t = \frac{1}{10}$ or $\frac{1}{5}$ is used to ensure a stable numerical solutions for the Grashof numbers considered in this study.

The wall vorticity is very important quantity and it is produced mainly at no-slip walls and then later advected and diffused into the rest of the flow. The wall vorticity boundary conditions are derived from the non-slip conditions [16, 17]. A first-order finite-difference form is used to approximate the wall vorticity ζ_w as:

$$\zeta_w = -2\frac{\psi_{w+1} - \psi_w}{\Delta n^2} + O(\Delta n). \quad (21)$$

Here, n is the direction normal to wall. The higher-order forms suffer from instability at high Grashof numbers. However, the first-order form is found to be the safest form to use and often gives results essentially equal to the higher-order forms. For this reason, the first-order form of the wall vorticity has been used throughout the calculations for the present work.

In a partially open enclosure, the difficulties encountered in specifying numerically the appropriate boundary conditions at the outflow have been discussed in refs. [9, 18–20]. The approach followed in the present work is based on the use of an extended computational domain outside the opening. It was first given by Kettleborough [21]. The outflow boundary conditions are applied at some distance sufficiently far away from the opening such that a further increase does not significantly alter the results obtained for the flow in the enclosure. The dimensions needed for such an extension beyond the opening are determined numerically. In this work, it was found that an extended computational domain of twice the height of the cavity is sufficient to produce an error of less than 0.1% for the mass outflow rate.

Finally, the computer code used for the present study was successfully validated by reference to a number of test cases that range from laminar to turbulent flow regimes. For more details see ref. [9].

3. RESULTS AND DISCUSSION

For the present study, the following parameters are held fixed at typical values of practical interest: the

height of the doorway opening $h_0 = 0.8$; and the initial location of the interface $h_i = 0.5$. Other values of the h_0 and h_i were also carried out. The results were found to be very similar to those presented here. The governing parameters of the problem are the Grashof number Gr and the stratification parameter $S = \Delta T_i/\Delta T_q$. In the present work, the influence of stratification parameter is explored for moderate Gr ($Gr = 2 \times 10^7$ and 2×10^8, laminar flow cases). The stratification parameter S is varied in the range from 0 to 1 for the given range of Gr. A value of S larger than 1 means that the ambient temperature rise is larger than the driving temperature difference $\Delta T_q = Q_0/\kappa$. These extreme cases of initial stratification of the ambient medium have no practical interest. For a given Gr, say $Gr = 2 \times 10^8$, $S < 0.1$ is a relatively weak stratification, while $S \geqslant 0.1$ is a stronger stratification. A steady state solution is sought, when one exists, by solving numerically the transient problem. The computed results are discussed in the following section.

3.1. *Transient behavior*

The numerical solution of the initial-value problem is carried out by marching in time until a steady state is reached. The achievement of a true steady state is made difficult by the presence of the internal gravity waves for values of $Gr \geqslant 2 \times 10^8$. For instance, at $Gr = 2 \times 10^7$ and lower, a steady state is reached after the oscillations are damped, as can be seen in Fig. 2(a), where the plot of Θ against time is given at one of the monitoring locations in the cavity ($x = 0.036$, $y = 0.5$), near the left wall. At $Gr = 2 \times 10^8$, for values of $S > 0$, oscillations were found to develop. These oscillations are shown in Fig. 2(b) for the temperature Θ at different values of the stratification parameter S. The oscillations become more pronounced as S is increased. This is indicated in Fig. 2. The amplitude of the temperature oscillations is very small, in fact, as small as 4×10^{-4} which is about 2.0% of the mean value of Θ. However its presence is not desirable and results in a tremendous increase in computer time since it becomes necessary to run the computer program for a long time to reach the steady state or periodic solutions.

It was not clear, at the beginning, if these oscillations were numerical or physical. They could be physical because of internal gravity waves, particularly when the medium is stratified. Therefore, calculations were performed with a refined grid. A sequence of non-uniform grids of 53×55 points (with 30×30 grid points inside the cavity) and 83×85 points (with 60×60 grid points inside the cavity) were used to ensure the grid independence of the computed oscillations. When oscillations are obtained, it is necessary to reduce the time step to check whether the oscillations still exist or not. Time steps of 0.5, 0.1 and 0.01 were used. In fact, starting from the initial condition of quiescent and thermal stratification (say $S = 0.14$), Θ evolves in an oscillatory fashion. By

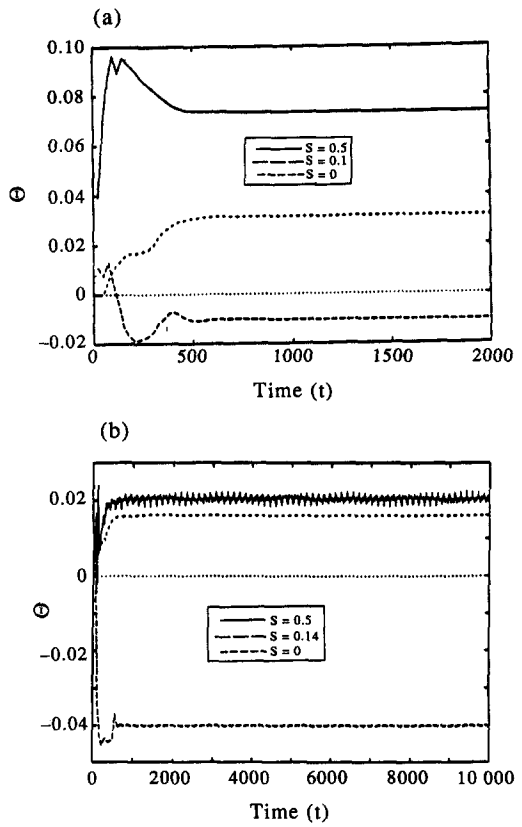

Fig. 2. The temporal development of the temperature Θ, at a given location ($x = 0.036$, $y = 0.5$), with various step ambient temperature stratifications. (a) $Gr = 2 \times 10^7$ and (b) $Gr = 2 \times 10^8$.

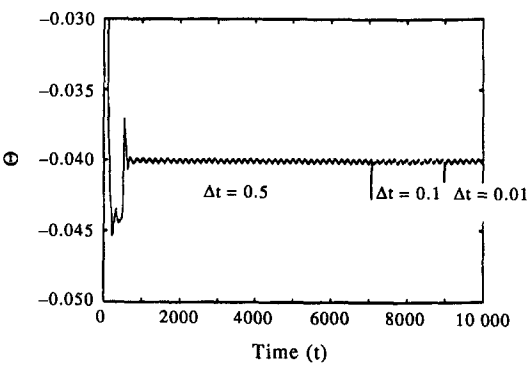

Fig. 3. The effect of time step on the temporal evolution of the temperature Θ for a step ambient temperature stratification ($S = 0.14$) at a given location $x = 0.036$, $y = 0.5$ inside the cavity and at $Gr = 2 \times 10^8$.

reducing the time step and recalculating, using the previous result as the initial approximation, the periodic nature (constant amplitude) of the oscillation becomes apparent. This is shown in Fig. 3. The frequency of this periodic motion is $N_0 = 3.13 \times 10^{-3}$, which is very close to the Brunt–Vaisala or buoyancy frequency [1]:

$$N_b = \frac{1}{2\pi}\sqrt{g\beta\frac{\partial T_{\infty,y}}{\partial y}}$$

for horizontally propagating gravity waves in a stably stratified fluid. In terms of the notation adapted for the present work, the buoyancy frequency is given by

$$N_b = \frac{\alpha}{2\pi H^2}(SGrPr^2)^{1/2} = 3.54\times 10^{-3}.$$

As the flow evolves two cells develop. The lower primary cell is due to the convective motion occurring in the lower layer. The other cell is a counter cell induced by the main or primary cell. As time proceeds, the main cell (i.e. the lower cell) achieves a steady state first, then the cell above it, as viscosity damps the internal gravity waves. The true steady state is obtained only after the two cells have stabilized. A similar behavior was observed by Musman [22] in his study of penetrative convection which depended on the density maximum of water near 4°C and by Torrance [7] in his study of natural convection flows induced by localized heating from below of a thermally stratified enclosure. In their calculations, both Musman and Torrance obtained oscillations, which they attributed to internal gravity waves.

3.2. *Influence of stratification*

Many experimental runs, with different Gr ranging from 10^6 to 2×10^8, were made to explore the effect of stratification. In each case with a fixed Gr, the stratification parameter S is varied from $S = 0.01$ to 0.5. For the sake of conciseness, the case with $Gr = 2\times 10^8$ is presented and discussed in detail to determine the influence of thermal stratification. Both step and linear ambient temperature profiles are examined, but due to lack of space only the results for the step ambient temperature case are presented. Furthermore, two extreme cases of ambient stratification are reported. The first case is for $0.1 < S \leqslant 0.5$, corresponding to a strong ambient temperature stratification and the second case is for $0 < S \leqslant 0.1$, corresponding to a relatively weak ambient temperature stratification. See ref. [9] for further details.

3.2.1. *Flow and thermal fields.* Figure 4 shows the variation of the steady state temperature and stream function with the stratification parameter S for a step ambient temperature distribution at $Gr = 2\times 10^8$. In Fig. 4, individual graphs from (a) to (b) pertain to a variation in S as $S = 0.05$ and 0.5. In each graph, the isotherms are plotted at the top frame and the stream function at the bottom frame. In these plots, the stream function ψ is scaled by $\sqrt{Gr}$ and the temperature Θ by $Gr\times 10^{-6}$. Both positive and negative temperature values appear in the contour plot. At a fixed height, positive temperature values indicate that the fluid element is hotter than the ambient medium at that particular height, whereas negative temperature values mean that the fluid is colder than the ambient at the same height.

The flow field reveals a multi-cellular pattern. This can be seen in the bottom frame in Fig. 4(a) and (b). There is one main or primary cell and a counter cell above it. The largest velocities are found in the main convective cell which extends from the lower boundary (floor) to the location where the vertical velocity of the wall plume drops to zero and then turns horizontally toward the opening. The maximum height of the turning point of the wall plume is defined here as the penetration height δ_p. The horizontal motion at the top of the main cell is towards the right, in the direction of the opening doorway, while the motion at the bottom of the main cell is towards the left, in the direction of the back wall. For the counter cell, it is the other way around. The flow in the main cell is caused by thermal buoyancy of the fluid inside the cavity, being warmer than the surrounding fluid outside the opening. In the upper part of the cavity, the temperature level is lower than that of the ambient medium at the same height. A counter-rotating cell is generated by the pressure difference due to the expansion of gases and the flow produced by the temperature difference between the upper region of the cavity and the ambient medium. The circulation and the velocities in the counter cell are substantially smaller than those in the main cell.

The convective motions occurring in the lower unstable region may penetrate into the upper stable region for a weaker stratification ($S \leqslant 0.1$, at $Gr = 2\times 10^8$). The penetration of convective motion takes place in the form of nearly horizontal flow in the bottom part of the stable layer, corresponding to the top part of the main cell, as indicated by the stream lines in Fig. 4. A behavior similar to this has also been reported by Musman [22] in his study of penetrative convection which depended on the density maximum of water near 4°C. Here, $S = 0.5$ corresponds to a strong ambient stratification and the penetration height of the main cell is obtained as $\delta_p = 0.37$ in the step ambient temperature variation case. A decrease in S intensifies the thermal plume and the amount of circulation in the main cell and, hence, increases the penetration height. For $S = 0.05$ or smaller, the plume hits the ceiling and a ceiling jet forms. See the review by Quintiere [23] and Jaluria and Cooper [24] for cases with behavior similar to this. In the absence of stratification, $S = 0$, a natural convection flow driven by the heat source is obtained. The results for such flows are given by Abib [9].

The isotherms plotted in the top frames of Fig. 4(a) and (b) display the influence of S on the plume development near the heat source. At smaller values of S, the thermal plume is well established near the heat source and is able to penetrate into the upper layer. However, at large values of S, the plume is confined to the lower-layer since it is unable to penetrate into the hot upper-layer. This is expected physically since the thermal stratification of the medium would affect the plume rise by lowering the tem-

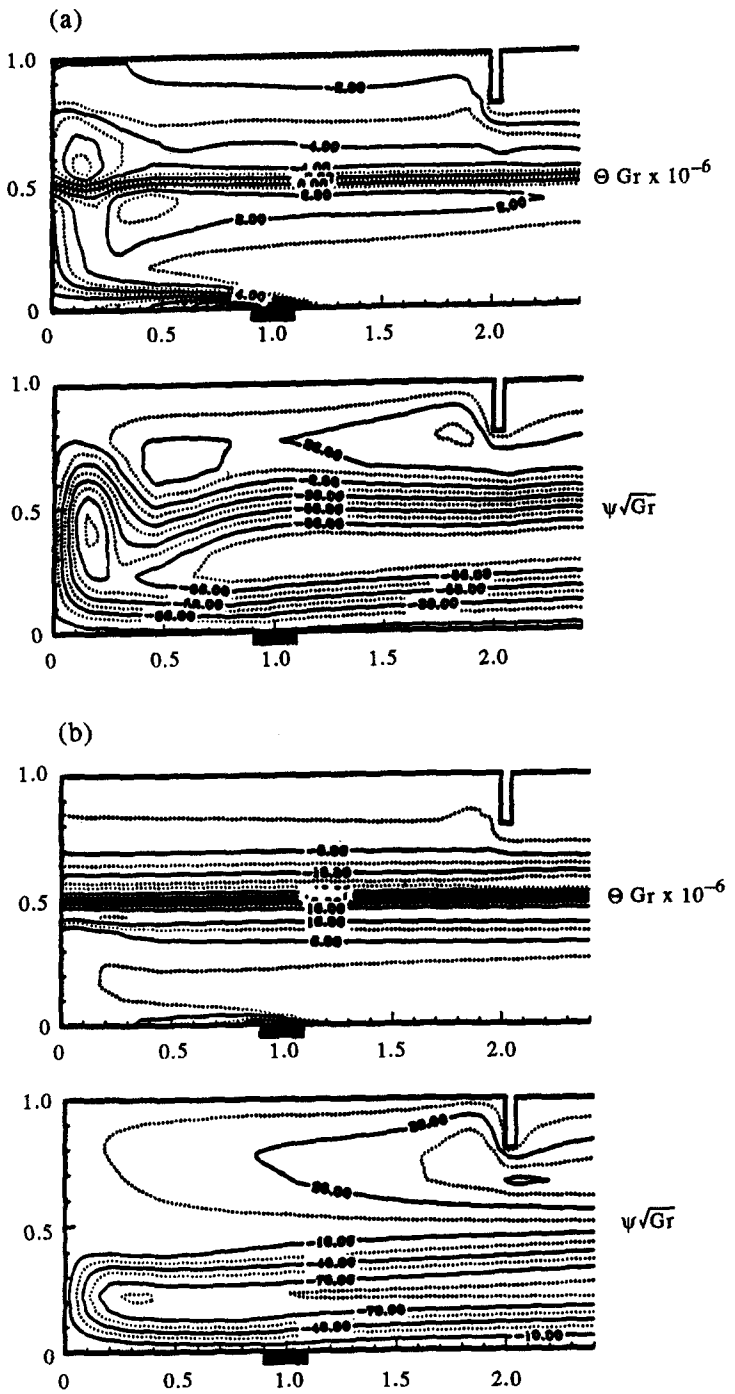

Fig. 4. Isotherms and streamlines at $Gr = 2 \times 10^8$ for step ambient temperature variations. (a) $S = 0.05$ and (b) $S = 0.5$.

perature difference between the fluid element and the ambient medium and, hence, the buoyancy force.

3.2.2. *Temperature profiles.* The vertical distribution of the computed temperature φ at three horizontal locations, namely $x = 0.5$, 1.0 and 2.0, for step ambient temperature stratifications, are plotted in Fig. 5(a). The same graph in terms of temperature Θ is also shown in Fig. 5(b) to show the local temperature distribution in reference to the temperature of the ambient medium. The figures illustrate the influence of S at $Gr = 2 \times 10^8$. In Fig. 5(a) the vertical variations of the temperature at different horizontal locations look similar, in particular, away from the walls and from the heat source. This means that the horizontal temperature gradients are small except in the thermal plume above the source. Three distinct regions can be

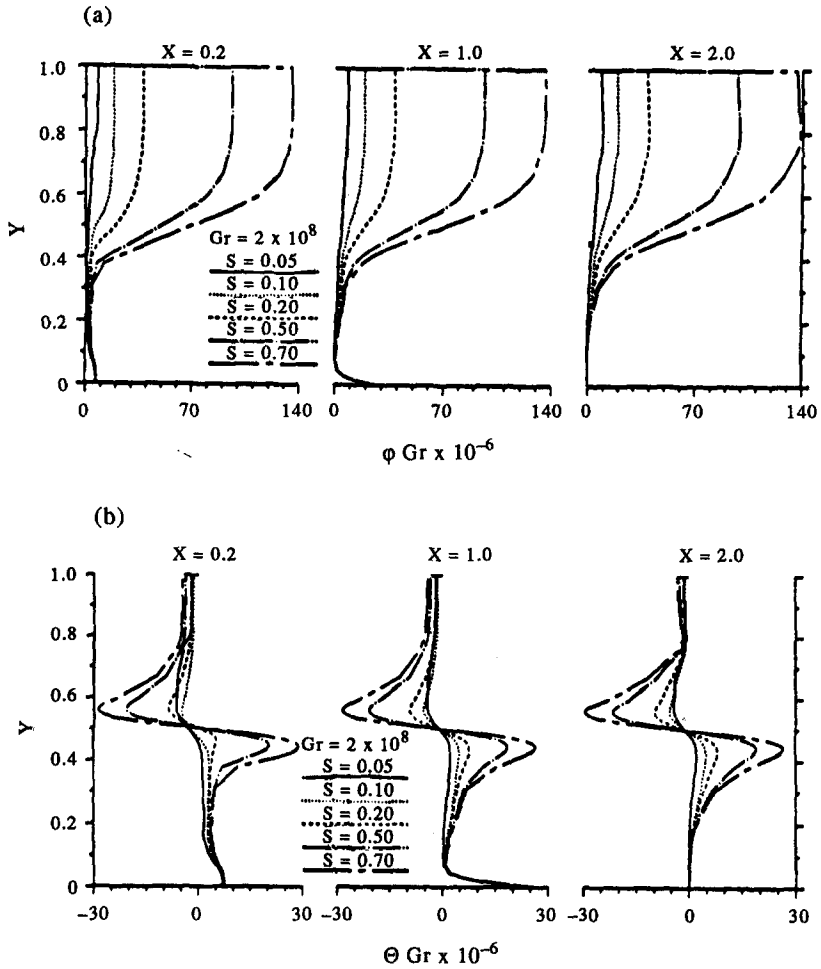

Fig. 5. The vertical distribution of the temperature, at $Gr = 2 \times 10^8$, for various step ambient temperature variations. (a) $\varphi = (T - T_{\infty,0})/(\dot{Q}_0/\kappa)$ and (b) $\Theta = (T - T_{\infty,y})/(\dot{Q}_0/\kappa)$.

identified from the vertical temperature profiles. These are the lower-layer, which is at a quasi-uniform temperature, the upper-layer which is also at a uniform temperature either at or lower than the ambient temperature, and the stratified layer in between the lower and upper layers. This middle stratified region is characterized by a presence of a local temperature defect and over-shoot, as can be seen in Fig. 5(b).

The influence of S on the thermal field can be analyzed by considering its effect on the above mentioned regions. For instance, at low values of $S < 0.1$ the temperature level is much lower and the thickness of the lower-layer is larger than the case of $S \geqslant 0.1$. This happens because, at $S < 0.1$, the thermal plume penetrates the upper stable layer to a certain degree. It is unable to reach the ceiling and merely turns back and spreads horizontally. This is due to the lack of enough thermal buoyancy to sustain the upward motion of the rising thermal plume. Thus, the plume establishes a recirculation within the upper- and lower-layers. It stirs and mixes the cooler lower-layer with fluid from the warmer upper-layer, which is at or slightly below the ambient temperature, thus causing the temperature level of the bottom part of the upper-layer to fall below the ambient value at that height. At the same time, the temperature level at the top part of the lower-layer rises above the ambient value. As a result of this, a stratified layer is established in between the lower-layer and the upper-layer as in Fig. 5(a) or a slight temperature defect and over-shoot appear at the interface as in Fig. 5(b).

3.2.3. *Velocity profiles and penetration distance.* The vertical distribution of the horizontal component of the velocity u is shown in Fig. 6 for different S values at three horizontal locations, namely $x = 0.5$, 1.0 and 2.0. The figure shows the influence of S at $Gr = 2 \times 10^8$. The u-velocity profiles show a strong convective main cell and a weaker counter cell above it. In the main cell, there is inflow of cooler fluid at the bottom of the cell and outflow of warmer fluid at the top part of the cell. The various curves collapse into an almost single curve at the bottom, while at the top of the main cell the effect of S is more pronounced. This is physically expected because at the bottom of the main cell (in the lower layer) the ambient temperature gradient is zero, whereas at the top of the cell, in

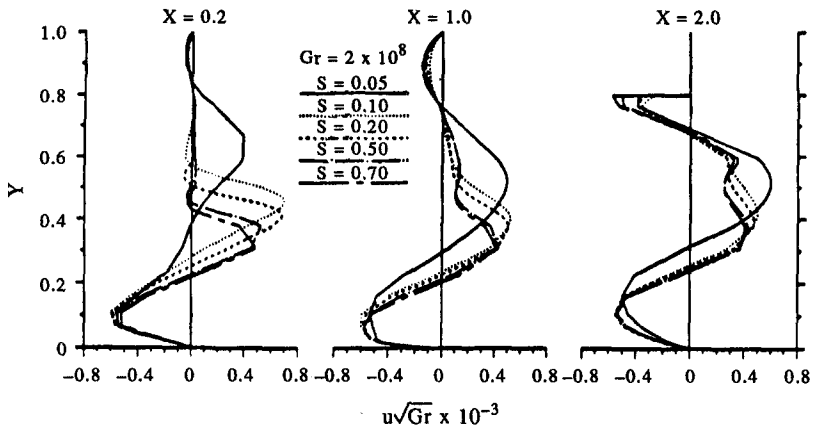

Fig. 6. The vertical distribution of the horizontal component of the velocity u, at $Gr = 2 \times 10^8$ for various step ambient temperature variations.

the vicinity of the interface, the ambient temperature gradient is large and, hence, the effect of S is more pronounced. The result is a decrease in the maximum horizontal velocity level u_{max} due to reduced thermal buoyancy as S increases. The vertical location of the u_{max} is also shifted towards the bottom surface as S increases. Note that penetration takes place in the form of horizontal motion at the top part of the main cell. Therefore, the penetration distance is computed as the maximum vertical location where the horizontal component of the velocity u in the top part of the main cell becomes zero. In other studies such as, for instance, that of Goldman and Jaluria [25] and Kapoor and Jaluria [26] in which wall flows and negatively buoyant ceiling jet has been investigated, the penetration distance is obtained by plotting the vertical temperature distribution and taking a sharp change in the profiles as indication of the extent of the penetration of the wall jet. The penetration distance obtained with the same criteria as that of Goldman and Jaluria involves a large margin of error (20–30%). This is because, as can be seen from the temperature profiles, there is no sharply defined change in the temperature profiles due to the presence of a stratified layer between the lower and the upper isothermal layers.

The penetration distance δ_p is plotted against the stratification parameter S in Fig. 7 for both step and linear ambient temperature profiles. The graph shows that, as the stratification parameter S is increased, the penetration distance decreases rapidly, for small values of S in the range $0 < S < 0.2$. It then slowly and almost linearly decreases for higher values of S corresponding to stronger stratification. At $S > 0.3$, the main cell is unable to penetrate into the stable upper layer. This is indicated by the fact that the corresponding δ_p is less than 0.45 (the location of the interfacial layer). One would expect that as S is increased beyond 0.5, the penetration distance would remain constant (for step profile), since the flow cannot penetrate into the upper stable layer. This does not happen because the increased stratification would not only decrease the buoyancy level of the main cell but it will also act as a source of energy. As a result, a counter cell is created above the main cell. This counter cell may grow in size and, therefore, the main cell has to adjust accordingly. Consequently the penetration distance of the main cell is lowered. In the case of the linear profile, this drop is more vigorous because the buoyancy is lowered even more due to the increasing ambient temperature with height.

3.2.4. *Heat transfer and mass outflow rates.* The influence of the stratification parameter S on the heat transfer and mass outflow rates is considered here. The average heat transfer rate at the source is given by the average Nusselt number based on the height of the cavity as

$$\overline{Nu} = \frac{\bar{h}H}{\kappa} = \frac{1}{l_s^2}\int_0^{l_s} \frac{1}{\Theta_s} dx. \tag{22}$$

Here l_s is dimensionless length of the source, $l_s = L_s/H$ and Θ_s is the dimensionless temperature at the surface of the source. H is the height of the cavity and is taken here as the characteristic length scale because it determines the size of the largest eddies in the vertical direction.

The effect of S on $\overline{Nu}$ is shown in Fig. 8(a) for step ($\diamond$) and linear ($+$) ambient temperature profiles. The solid and broken lines curves in Fig. 8(a) are obtained by a least-squares curve fit. The figure shows that, in a linear profile, as S is increased the Nusselt number decreases slowly at the smaller value of S and at a higher rate for larger values of S. On the contrary, the Nusselt number does not vary much in the case of the step profile. The variation is less than 2.5–3.0%. This happens because, in the case of linear profile, the ambient temperature varies with height and, therefore, the local temperature difference between the source and the ambient medium is smaller. This results in lower velocities, smaller mass flow rate and lower heat transfer rate. In the step profile, the ambient

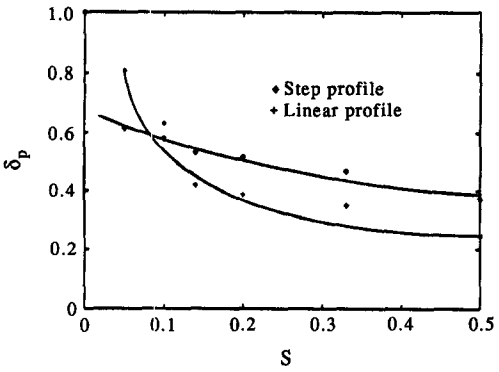

Fig. 7. Penetration distance δ_p vs the stratification parameter S, at $Gr = 2 \times 10^8$. The symbols are the results from numerical solutions. The lines are obtained by a least-squares curve fit.

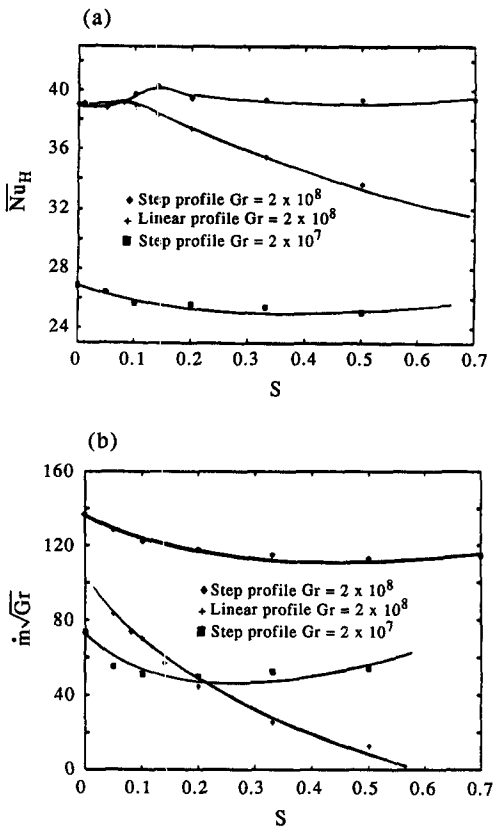

Fig. 8. (a) Average Nusselt number $\overline{Nu}$ and (b) average mass outflow rate $\dot{m}$ vs the stratification parameter S at $Gr = 2 \times 10^8$. The symbols are the results from numerical solutions. The lines are obtained by a least-squares curve fit.

temperature varies with height only in the vicinity of the interface. The main convective cell which is responsible for most of the flow and the thermal pattern is confined to the lower-layer where the ambient temperature gradient is zero. Therefore, the effect of S on the heat transfer and the flow rates is small.

Figure 8(b) shows the mass outflow rate at the opening vs S for step ($\diamond$) and the linear ($+$) ambient temperature profiles. The mass outflow rate decreases with an increase of S in both cases. This is physically expected because stratification can be viewed as an impediment to the flow in the sense that the stratification reduces the buoyancy level and, hence, results in lower velocities and smaller mass flow rates.

4. CONCLUSIONS

A penetrative convection, in a partially open enclosure heated from below by a localized energy source and with stably stratified ambient medium, has been studied. The study mainly focused attention on the interaction between the open cavity and the environment due to the temperature stratification of the ambient medium for moderate Gr.

In the range of the stratification parameter S examined, it was found that for small values of S the thermal plume reaches the ceiling, while for large values of S it is unable to penetrate into the stable upper-layer. The flow exhibits a multi-cellular pattern consisting of a main convective cell at the bottom part of the cavity and a weak counter cell at the top. The penetrative flow takes places in the form of horizontal motion in the lowest part of the stable upper-layer which corresponds to the top part of the main cell. The thermal stratification reduces the buoyancy level and, hence, results in lower velocities, smaller mass flow rates, lower heat transfer rates, and lower penetration distances.

Acknowledgements—The authors acknowledge the partial support provided by the Building and Fire Research Laboratory, National Institute of Standards and Technology, under grant no. 60NANB7D0743 for this work.

REFERENCES

1. J. S. Turner, *Buoyancy Effects in Fluids*. Cambridge University Press, London (1973).
2. B. J. McCaffrey and J. G. Quintiere, Buoyancy driven countercurrent flow generated by a fire source. In *Heat Transfer and Turbulent Buoyant Convection* (Edited by D. B. Spalding and N. Afgan), Vol. II, pp. 457–472. Hemisphere, Washington, DC (1977).
3. Y. Jaluria, *Natural Convection Heat and Mass Transfer*. Pergamon Press, London (1980).
4. E. J. List, Turbulent jets and plumes, *A. Rev. Fluid Mech.* **14,** 189 (1982).
5. G. Walin, Contained non-homogeneous flow under gravity or how to stratify a fluid in the laboratory, *J. Fluid Mech.* **48,** 647 (1971).
6. C. F. Chen, D. B. Briggs and R. A. Wirtz, Stability of thermal convection in a salinity gradient due to lateral heating, *Int. J. Heat Mass Transfer* **14,** 57 (1971).
7. K. E. Torrance, Natural convection in thermally stratified enclosures with localized heating from below, *J. Fluid Mech.* **95,** 477 (1979).
8. L. Y. Cooper, M. Harkleroad, J. G. Quintiere and R. Rinkinen, An experimental study of upper hot layer stratification in full-scale multiroom fire scenario, *J. Heat Transfer* **104,** 741 (1982).
9. A. H. Abib, Penetrative and recirculating flows in enclosures with openings, Ph.D. Thesis, Rutgers University, New Brunswick, NJ (1992).

10. S. V. Patankar, *Numerical Heat Transfer and Fluid Flow*. Hemisphere, Washington, DC (1980).
11. D. Peaceman and H. Rachford, The numerical solution of parabolic and elliptic differential equations, *J. Soc. Ind. Appl. Math.* **3,** 28–41 (1955).
12. J. Douglass and J. E. Gunn, A genereal formulation of alternating direction implicit method I. Parabolic and hyperbolic problem, *Numerische Mathematik* **6,** 428–453 (1964).
13. I. P. Jones, The convergence of a simple iterative strategy for strongly stratified flows. In *Numerical Methods on Laminar and Turbulent Flow* (Edited by C. Taylor), p. 733. Pineridge Press, Swansea (1985).
14. C. P. Thompson, N. S. Wilkes and I. P. Jones, Numerical studies of buoyancy-driven turbulent flow in a rectangular cavity, *Int. J. Numer. Meth. Engng* **24,** 89 (1987).
15. R. A. W. M. Henkes, Natural convection boundary layers, Ph.D. Thesis, Delft University, Delft, Netherlands (1990).
16. P. J. Roache, *Computational Fluid Dynamics*. Hermosa Publishers, Albuquerque, NM (1972).
17. R. Peyret and D. Taylor, *Computational Methods for Fluid Flow*. Springer, New York (1983).
18. P. Le Quere, J. A. C. Humphrey and F. S. Sherman, Numerical calculation of thermally driven two-dimensional unsteady laminar flow in cavities of rectangular cross section, *Numer. Heat Transfer* **4,** 249–283 (1981).
19. F. Penot, Numerical calculation of two-dimensional natural convection in isothermal open cavities, *Numer. Heat Transfer* **5,** 421–437 (1982).
20. Y. L. Chan and C. L. Tien, Numerical study of two-dimensional laminar natural convection in shallow open cavities, *Int. J. Heat Mass Transfer* **28,** 603–612 (1985).
21. C. F. Kettleborough, Transient laminar free convection between heated vertical plates including entrance effects, *Int. J. Heat Mass Transfer* **15,** 883–896 (1972).
22. S. Musman, Penetrative convection, *J. Fluid Mech.* **31,** 343 (1968).
23. J. G. Quintiere, Perspective on compartment fire growth, *Combust. Sci. Technol.* **39,** 11 (1984).
24. Y. Jaluria and L. Y. Cooper, Negatively buoyant wall flows generated in enclosure fires, *Proc. Energy Combust. Sci.* **15,** 159–182 (1989).
25. D. Goldman and Y. Jaluria, Effect of opposing buoyancy on the flow in free and wall jet, *J. Fluid Mech.* **166,** 41 (1986).
26. K. Kapoor and Y. Jaluria, Penetrative convection of a plane turbulent wall jet in a two-layer thermally stratified environment: a problem in enclosure, *Int. J. Heat Mass Transfer* **36,** 155 (1993).